Available online at www.sciencedirect.com
SCIENCE DIRECT
Journal of Catalysis 235 (2005) 150–163
JOURNAL OF CATALYSIS
www.elsevier.com/locate/jcat

New Fe/SiO_2 materials prepared using diiron molecular precursors: Synthesis, characterization and catalysis

Andrew W. Holland [a,b], Guangtao Li [a,b], Ahmed M. Shahin [c], Gary J. Long [c], Alexis T. Bell [b,d], T. Don Tilley [a,b,*]

[a] *Department of Chemistry, University of California, Berkeley, CA 94720-1461, USA*
[b] *Chemical Sciences Division, Lawrence Berkeley National Laboratory, 1 Cyclotron Road, Berkeley, CA 94720, USA*
[c] *Department of Chemistry, University of Missouri-Rolla, Rolla, MO 65409-0010, USA*
[d] *Department of Chemical Engineering, University of California, Berkeley, CA 94720-1462, USA*

Received 21 April 2005; revised 1 July 2005; accepted 7 July 2005

Available online 25 August 2005

Abstract

Several well-defined diiron siloxide complexes have been synthesized, isolated, characterized, and used as molecular precursors for the grafting of well-defined isolated iron species on the surface of mesoporous silica SBA-15. The precursors have bridging siloxide ligands, a diamine linker, or a μ–oxo diiron core, and their binuclear structures have been confirmed by elemental analysis, solution molecular weight measurements, and nuclear magnetic resonance spectroscopy. All precursors react with SBA-15 to immobilize the iron centers and produce silanol; the various stoichiometries and structural implications of these grafting reactions are discussed. Calcination of the grafted iron complexes yields materials largely devoid of organic components, and these calcined catalysts are active in the oxidation of hydrocarbons by hydrogen peroxide. The catalytic activities and selectivities of these materials are compared with each other and with those of other Fe/SiO_2 catalysts. Issues including iron-loading dependence and grafting conditions are discussed. Characterization of the catalysts by diffuse–reflectance ultraviolet–visible, X-band electron paramagnetic resonance, Mössbauer, and extended X-ray absorption fine structure spectroscopies indicates that although the diiron structures of the precursors are usually maintained during the initial grafting process, calcination results in their conversion to monoiron centers on the support. This theory is also consistent with the generally similar catalytic behaviors of materials prepared from diiron and monoiron precursors. The implications of these findings for the generality of molecular precursor techniques are discussed.

Keywords: Molecular precursors; Hydrocarbon oxidation; Fe/SiO_2; Diiron centers

1. Introduction

Iron centers supported on inorganic oxides constitute a promising class of catalysts for the selective oxidation of hydrocarbons. Most prominently, iron-exchanged zeolites (Fe-ZSM-5) have proven to be uniquely effective catalysts for the monohydroxylation of benzene by N_2O under relatively mild conditions [1,2]. To date, the structure of these catalysts' active "α" sites remains a subject of vigorous debate; reports have proposed that the catalysis may occur at monoiron centers [3], diiron sites [4], or even larger iron clusters isolated within the zeolite matrix [5]. Both monoiron and diiron sites feature prominently in biological oxidation chemistry [6–15]; the development of synthetic mimics of iron-based oxidation enzymes for use as models and oxidation catalysts has been a subject of intense study for decades [16–24]. As such, the synthesis of related iron species in the context of a heterogeneous catalyst presents unique opportunities both to investigate diiron centers from a new perspective and to apply our knowledge of solution-phase systems

* Corresponding author.
E-mail address: tdtilley@berkeley.edu (T.D. Tilley).

0021-9517/$ – see front matter
doi:10.1016/j.jcat.2005.07.003

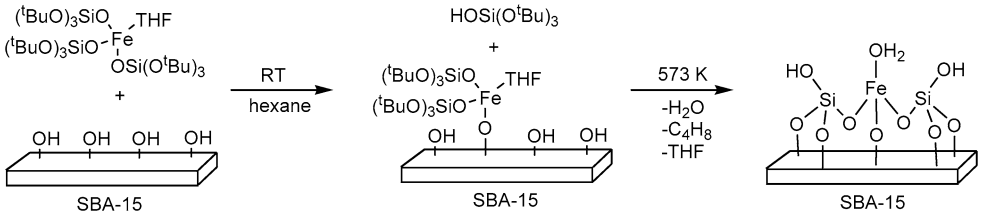

Scheme 1.

to the understanding and improvement of the heterogeneous catalysts.

Many questions remain regarding fundamental characteristics of Fe-zeolite catalytic systems. A large body of knowledge regarding these catalysts has been compiled over many years of theoretical [25,26], spectroscopic [27–35], and microscopic [29,35] investigations of these materials, but these studies have yet to forge a consensus regarding the structure of the active catalyst. Findings from extended X-ray absorption fine structure (EXAFS) [36,37] and Mössbauer [27,31,34,38–40] spectroscopies have suggested the presence of both monoiron and diiron centers, and some studies have even demonstrated correlations between catalytic activity and specific spectroscopic features [34]. X-band electron paramagnetic resonance (EPR) spectroscopy [39,41] and transmission electron microscopy [29,42] have been used to follow the state of iron over the course of activation procedures, and the extra-framework iron (rather than framework iron or bulk iron oxide) have been identified as being crucial to catalytic activity. Nonetheless, conflicting results have frustrated the development of any widespread agreement regarding the specific structure of the active site.

A major obstacle to the unambiguous characterization of supported iron centers lies in the limitations of the methods conventionally used in their syntheses. Common approaches offer little rational control over the molecular detail of a material's structure, and thus no means of independently preparing and investigating proposed active structures. Iron is generally introduced to inorganic oxides as a simple inorganic salt [43–46], either during support synthesis or thereafter, and the active catalyst is prepared by subjecting the resulting material to steaming at high temperature [2,47]. Many studies have demonstrated the importance of this activation process, but it appears to serve chiefly to facilitate adoption of the most thermodynamically favorable iron distribution [28,31,34,35,42]. These methods thus offer no means by which to control the specific structure of the iron sites, and thus no opportunity to systematically compare the reactivities of the different structures proposed as active sites. Current methods also generally require the use of relatively low loading regimes to guarantee site isolation [48], which has been demonstrated to be a key to activity in many catalytic systems [49–52]. By overcoming these limitations, new methods allowing for the direct control of active site structure at the molecular level would pave the way for useful investigations and the rational preparation of improved materials.

One such method is the use of molecular precursors, wherein carefully designed metal complexes are introduced to the support under conditions in which they retain their original structure. There is growing evidence that this technique can be useful in the controlled preparation of well-defined inorganic materials [53–58]. We recently reported the application of such an approach to the preparation of strictly isolated monoiron centers on mesoporous silica SBA-15 [59] (chosen for its large pores and relatively simple surface structure) [60]. Introduction of the bulky iron siloxide complex (THF)Fe[OSi(O^tBu)$_3$]$_3$ (**1a**) to a hydroxylic support results in the attachment of iron atoms to the surface through the formation of new Fe–O bonds (and concomitant liberation of silanol) (Scheme 1). Subsequent calcination yields an inorganic catalyst active in the oxidation of hydrocarbons by hydrogen peroxide. Initial spectroscopic investigations and more recent EXAFS studies [61] have demonstrated that the iron centers are isolated. This structural feature can be credited both to the bulky structure of the precursor and to the clean, mild, nonaqueous conditions of its grafting. Formation of isolated iron centers in this system is an outcome that stands in marked contrast to the results of conventional impregnation conducted at similar iron loadings; materials prepared by the latter route contain substantial amounts of bulk iron oxide [43–46], as do all known Fe/SiO_2 materials subjected to high-temperature steaming [38,62,63]. Thus, the molecular precursor approach affords a material with an iron distribution subject to kinetic control and permits tuning of the local iron structure through precursor design.

As an extension of our work on isolated monoiron catalysts, we sought to prepare and graft diiron precursors to investigate the stability and oxidation activity of isolated diiron centers on oxide surfaces. μ–Oxo diiron centers are also ubiquitous in homogeneous oxidation systems of both biological [7,9,10] and synthetic [64,65] origin. Herein we report the results of efforts to support diiron centers on mesoporous silica using the molecular precursor technique, and the catalytic behavior of the resulting materials.

2. Experimental

2.1. General procedures

Unless otherwise indicated, all procedures were carried out under nitrogen atmosphere using standard Schlenk tech-

niques and/or an inert-atmosphere glovebox. All solvents and liquid reagents were purified and distilled according to standard procedures. Other materials were purchased from commercial suppliers and used as received, except for $Fe[N(SiMe_3)_2]_2$ [66], $HOSi(O^tBu)_3$ [67], $(^tBuO)_3SiONa$ [68], $[(^tBuO)_3SiO]_3Fe(THF)$ [60], $[Cl_3FeOFeCl_3][NEt_4]_2$ [69], and SBA-15 [59], which were prepared according to published procedures.

Surface area measurements were performed by the BET method as implemented by a Quantachrome surface area analyzer. SBA-15 surface hydroxyl group densities were measured by nuclear magnetic resonance (NMR) analysis of the deprotonation of SBA-15 by $MgBn_2(THF)_2$ [70], and also by thermogravimetric analysis (TGA) [71]; reported values correspond to an average of these two results, which always agreed to within 15%. Solution molecular weight measurements were conducted by the Signer method [72,73]. All NMR experiments were conducted using ferrocene as an internal standard. Elemental analyses were performed at the microanalytical facility in the College of Chemistry, University of California Berkeley (C, H, N) or at Galbraith Analytics (Fe). Diffuse–reflectance UV–visible spectra were recorded using a Varian-Cary 14 spectrophotometer equipped with a Harrick diffuse–reflectance attachment. MgO was used as a reference. EPR spectroscopy was performed under nitrogen at ambient temperature using a Bruker EMX spectrometer. Infrared spectra were recorded on a Mattson Instruments Galaxy 3000 Fourier transform spectrometer.

Fe K-edge XAS measurements (EXAFS spectra) for all the samples were performed at beamline 6–2 of the Stanford Synchrotron Radiation Laboratory (SSRL) and beamline X11A of the National Synchrotron Light Source (NSLS) in a transmission mode. Both beamlines were equipped with a Si(111) double-crystal monochromator. Iron metal foil (7 µm) was used to calibrate the X-ray energy. Each sample was pressed as a rectangular wafer (0.43 × 1.86 cm, with the thickness depending on the amount of sample used) and then loaded into a specially designed sample holder for XAS measurements. Appropriate amounts of samples were used (typically 5–10 mg for standards and 80–100 mg for supported iron materials) based on a calculated absorption length ($\mu_m \rho x$) of 2. The sample holder was put under vacuum (10^{-6} Torr) before each measurement. During the measurements, the sample holder was kept at 77 K (liquid nitrogen temperature) to minimize the thermal noise. Intensities of the beam were measured over a 900-eV range. Ionization chambers (N_2 filled) were used to measure the incident (I_0) and sample transmitted (I_1) fluxes. Between three and five scans were taken for each sample to further improve the signal-to-noise ratio. Normalization and extraction of the EXAFS data were done with the aid of IFEFFIT integrated program. All spectra were transformed with a Hanning window function using a windowsill (dk) of 1 $Å^{-1}$ centered on the chosen nodal position. The scattering function $\chi(k)$ was multiplied by k^3 and then Fourier-transformed without phase correction.

Mössbauer spectra were measured at 77 K on a constant-acceleration spectrometer that used a room-temperature rhodium matrix cobalt 57 source and was calibrated at room temperature with α-iron foil. The estimated absolute errors, unless otherwise indicated, are ±0.01 mm/s for the isomer shifts and ±0.02 mm/s for the quadrupole splittings and line widths. All spectral absorbers were prepared and manipulated in an inert atmosphere. The absorbers were placed, under nitrogen, in the vacuum chamber of a liquid nitrogen cryostat that was subsequently evacuated and cooled to 77 K. Thus the samples were protected by a vacuum at all times during acquisition of the spectra.

Thermal analysis was conducted using a Dont model 2000 TGA/DSC system. Gas chromatography (GC) was performed with an Agilent 6890 series GC system using an HP-1 methylsiloxane capillary column (50 m × 320 µm × 1.05 µm nominal), integration was performed relative to an n-dodecane internal standard. NMR spectroscopy was performed at ambient temperature using a Bruker AMX 400 spectrometer (400 MHz).

2.2. Precursors syntheses

2.2.1. $\{Fe[OSi(O^tBu)_3]_2\}_2$ (**2**, Eq. (1))

$Fe[N(SiMe_3)_2]_2 + (^tBuO)_3SiOH$

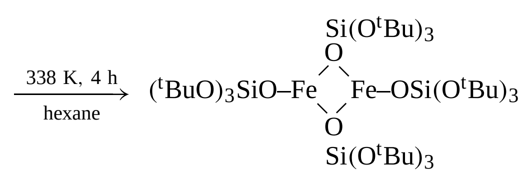

2 (1)

A Schlenk tube was charged with $Fe[N(SiMe_3)_2]_2$ (1.8 g, 4.8 mmol), $HOSi(O^tBu)_3$ (2.65 g, 10.0 mmol), hexane (50 mL), and a teflon-coated stirbar. The resulting yellow-green solution was stirred at 333 K for 1 h, during which the color of the solution bleached to pale brown. The solvent was then removed in vacuo, and the residual silanol was removed by sublimation at 343 K under dynamic vacuum. The remaining off-white solid was then crystallized from pentane (5 mL) at 193 K to yield blocky off-white crystals of **2** (2.25 g, 80% yield). Thorough removal of free silanol was critical to successful crystallization of the product. ^1H NMR (benzene-d_6, 295 K): 5.21 (br, 9H), −11.23 (br, 9H) ppm. IR (Nujol, cm^{-1}): 1365 (m), 1243 (m), 1190 (m), 1065 (s), 1027 (w), 972 (m), 828 (w). mp 450–452 K (dec.). Anal. Calcd for $C_{48}H_{108}Fe_2O_{16}Si_4$: C, 49.5; H, 9.34. Found: C, 49.7; H, 9.50. Solution molecular weight calcd for $C_{48}H_{108}Fe_2O_{16}Si_4$: 1164. Found: 1140.

2.2.2. $Fe[OSi(O^tBu)_3]_3(Et_2O)$ (**1b**)

A glass bomb was charged with anhydrous $FeCl_3$ (0.230 g, 1.42 mmol), $NaOSi(O^tBu)_3$ (1.22 g, 4.26 mmol), diethylether (50 mL) and a stirbar. The heterogeneous mixture was

stirred at 348 K for 48 h, after which it was pale brown in appearance. The volatile materials were removed in vacuo, and the resulting off-white solid was extracted into pentane (20 mL). Crystallization from pentane (5 mL) at 243 K yielded **1b** as very pale green blocks (0.53 g, 40% yield). Mp 411–412 K (dec.). Anal. Calcd for $C_{40}H_{91}FeO_{13}Si_3$: C, 52.2; H 9.97. Found: C, 52.0; H, 9.87.

*2.2.3. [(tBuO)3SiO]3Fe(NMe2C2H4NMe2)Fe[OSi(OtBu)3]3 (**3a**, Eq. (2))*

$$[(^tBuO)_3SiO]_3Fe(OEt_2) + Me_2N(CH_2)_2NMe_2 \xrightarrow[\text{toluene}]{295\ \text{K},\ 3\ \text{h}}$$

1a

$$[(^tBuO)_3SiO]_3Fe\text{–}N(Me_2)\text{–}CH_2\text{–}CH_2\text{–}N(Me_2)\text{–}Fe[OSi(^tBu)_3]_3 \quad (2)$$

3a

In a typical experiment, a Schlenk tube was charged with **1b** (0.24 g, 0.26 mmol), toluene (10 mL), and a stirbar. A toluene solution of *N*,*N*,*N*′,*N*′-tetramethyl-ethylenediamine (20 μL, 0.13 mmol) was then added dropwise while stirring, resulting in immediate bleaching of the pale yellow solution to colorless. The volatile materials were removed in vacuo, and the resulting pale solid was crystallized from pentane (3 mL) at 243 K to afford **3a** as off-white plates (0.21 g, 89%). ^{1}H NMR (benzene-d_6, 295 K): no signal observed. IR (Nujol, cm^{-1}): 1364 (m), 1243 (m), 1194 (m), 1054 (s), 1024 (w), 979 (s), 827 (w). Mp 493 K (dec.). Anal. Calcd for $C_{78}H_{178}O_{24}N_2Fe_2Si_6$: C, 51.80; H, 9.92; N, 1.59. Found: C, 51.86; H, 10.05; N, 1.55. Solution molecular weight Calcd for $C_{78}H_{178}O_{24}N_2Fe_2Si_6$:1806. Found: 1830. $[(^tBuO)_3SiO]_3Fe(NMe_2C_3H_6NMe_2)Fe[OSi(O^tBu)_3]_3$ (**3b**). Anal. Calcd for $C_{79}H_{180}O_{24}N_2Fe_2Si_6$: C, 52.06; H, 9.95; N, 1.54. Found: C, 52.09; H, 10.17; N, 1.60. Mp 483 K (dec.). $[(^tBuO)_3SiO]_3Fe(NMe_2C_4H_8NMe_2)Fe[OSi(O^tBu)_3]_3$ (**3c**). Anal. Calcd for $C_{80}H_{182}O_{24}N_2Fe_2Si_6$: C, 52.32; H, 9.98; N, 1.50. Found: C, 52.36; H, 10.16; N, 1.59. Mp 488–493 K (dec.).

*2.2.4. [NEt4]2{[(tBuO)3SiO]3FeOFe[OSi(OtBu)3]3} (**4**, Eq. (3))*

$$[NEt_4]_2[(Cl_3Fe)_2O] + (^tBuO)_3SiONa \xrightarrow[\text{THF}]{295\ \text{K},\ 20\ \text{h}}$$

$$[NEt_4]_2\{[(^tBuO)_3SiO]_3Fe\text{–}O\text{–}Fe[OSi(O^tBu)_3]_3 \quad (3)$$

4

A Schlenk tube was charged with $[FeCl_3OFeCl_3][NEt_4]_2$ (0.46 g, 0.77 mmol), $NaOSi(O^tBu)_3$ (1.32 g, 4.61 mmol), and a stirbar, and THF (100 mL) was added with stirring. The resulting suspension was stirred at 295 K for 20 h, during which it took on a yellow color and a pale precipitate formed. The volatile materials were removed in vacuo, and the resulting orange solid was extracted with pentane (2 × 50 mL). The volume of the extract was reduced to 5 mL in vacuo, and crystallization of this solution at −193 K yielded **4** as yellow orange crystals (0.71 g, 47% yield). ^{1}H NMR (benzene-d_6, 295 K): no signal observed. IR (Nujol, cm^{-1}): 1363 (m), 1240 (m), 1194 (m), 1050 (s), 1024 (w), 984 (s), 824 (m). Mp 462–463 K (dec.). Anal. Calcd for $C_{88}H_{202}Fe_2N_2O_{25}Si_6$: C, 53.69; H, 10.34; N, 1.42. Found: C, 53.51; H, 10.28; N, 1.29. Solution molecular weight Calcd for $C_{88}H_{202}Fe_2N_2O_2Si_6$: 1969. Found: 1870.

2.3. Catalysts and catalysis

2.3.1. Catalyst preparation

Typically, 393 K-dried SBA-15 (0.40 g; 875 m^2/g, 1.1 SiOH/nm^2, 0.64 mmol SiOH) was suspended in hexane (40 mL) by stirring for 2 h. The appropriate precursor (**2**, 0.062 g, 0.053 mmol) was then introduced as a hexane solution (10 mL), and stirring was continued for 20 h at 295 K. The solid material was then collected by filtration, washed with hexane (40 mL), and dried in vacuo to yield uncalcined catalyst **2-SBA15$_{295}$** (425 mg, 95% yield). Subsequently, this material was calcined under oxygen (usually at 573 K for 2 h after a 5-K/min temperature ramping). The resulting material (**2-SBA15$_{573}$**) was analyzed for surface area and C, H, and Fe content. Catalysts were dried under vacuum at 150 °C before use or characterization. Exposure to water vapor did not affect the catalytic or spectroscopic properties of catalysts, provided that the catalyst was subsequently dried before use.

2.3.2. Catalysis

Typically, a 50-mL Schlenk flask was loaded with the calcined, dried catalyst (40 mg), acetonitrile (5.0 mL), benzene (2.0 mL, 22.4 mmol), and dodecane (20 μL, 0.21 mmol). This mixture was stirred for several minutes at 333 K, after which hydrogen peroxide (30% $H_2O_{2(aq)}$, 0.41 mL, 4.0 mmol) was introduced. Aliquots (0.1 mL) were collected, filtered, and analyzed by GC at regular intervals. Toluene oxidation was conducted at 333 K using 22.4 mmol of toluene; adamantane oxidation was performed at 333 K using 5.6 mmol of substrate; and cyclohexane oxidation was conducted at 298 K using 18.5 mmol of substrate and 0.021 mmol of dodecane. Catalytic results are listed in Tables 2 and 4.

3. Results

3.1. Catalyst preparation: grafting and calcination

Table 1 lists the equivalents of $HOSi(O^tBu)_3$ and isobutylene released per dimer molecule during the grafting of precursors **2**, **3**, and **4** by treating a hexane suspension of SBA-15 with a hexane solution of the precursor. Monitoring of these reactions by ^{1}H NMR revealed that the nature of the grafting reaction depended on the precursor investigated. Grafting of precursor **2** yielded 2 equivalents of

Table 1
Characteristics of catalysts prepared by grafting at 295 K for 20 h[a]

Entry	Catalyst precursor	Surface area (m^2/g)	OH (nm^{-2})	%Fe	Fe (nm^{-2})	Silanol Equiv/Fe_2	C_4H_8 Equiv/Fe_2	%C (calc)	%H (calc)
1[b]	**1a**	875	1.1	1.90	0.23	1.0	0.1	10.9 (11.4)	1.9 (2.1)
2	**2**	650	1.4	3.14	0.52	1.9	0	9.0 (8.1)	1.7 (1.5)
3	**2**	530	3.3	2.69	0.54	2.0	0.1	7.75 (6.93)	1.7 (1.3)
4	**2**	650	1.4	1.24 (1.20)	0.19	1.9	0	3.43 (3.55)	0.89 (0.66)
5	**3a**	800	1.3	2.20	0.29	0.9	1.2	11.6 (11.9)	2.7 (2.3)
6	**3a**	660	3.8	*2.01*	*0.32*	1.0	1.3	12.9 (*13.3*)	2.4 (*2.5*)
7[c]	**3a**	800	1.3	*2.25*	*0.30*	1.2	1.8	13.9 (*15.0*)	2.5 (*2.9*)
8	**3a**	825	1.4	1.21 (1.25)	0.16	1.0	1.2	8.82 (9.02)	2.1 (2.0)
9	**3b**	800	1.3	*2.10*	*0.28*	0.9	1.4	13.8 (*14.1*)	2.6 (*2.6*)
10	**3c**	800	1.3	*2.05*	*0.28*	1.1	1.2	13.2 (13.6)	2.2 (*2.6*)
11	**4**	800	1.4	1.95	0.26	1.0	1.2	12.8 (13.4)	2.7 (2.8)
12	**4**	660	3.8	1.67	0.27	1.0	1.3	10.4 (11.4)	2.2 (2.5)
13[c]	**4**	825	1.4	*1.99*	*0.26*	1.3	1.9	11.9 (13.5)	2.3 (2.8)
14	**4**	825	1.4	1.24 (1.30)	0.16	1.1	1.4	7.54 (7.80)	1.6 (1.6)

[a] Samples were prepared at maximum iron loading (see text) unless a theoretical value is given in parentheses. All values in parentheses are predicted based on observed or intended stoichiometry. Values in italics are extrapolated from NMR observations rather than measured by microanalysis.
[b] Results taken from Ref. [60].
[c] Materials subjected to grafting conditions for 48 h, rather than 20 h.

$HOSi(O^tBu)_3$ per dimer molecule, or 1 equivalent per iron center (entries 2–4). This reaction proceeded with a half-life of 4–5 h, and was accompanied by no detectable production of isobutylene or other byproducts. In contrast, both precursors **3** and **4** reacted rapidly with an excess of SBA-15 to yield 1 equivalent of silanol per molecule within 1 h of mixing. These reactions went on to afford 1–2 equivalents of isobutylene, as well as small amounts of additional silanol and ^{t}BuOH, over the subsequent 20 h (entries 5–14). In no cases were any other products observed.

The carbon, hydrogen, and iron compositions of the grafted materials **2–4-SBA15$_{295}$** were consistent with the spectroscopic observations described earlier, with C and H contents reduced under conditions that yielded more isobutylene. The upper limits of iron loading, probed by adding a large excess of molecular precursor and washing extensively after grafting, varied significantly among the catalysts. The iron(II) precursor **2** yielded 3.1% Fe incorporation, the TMEDA bridged precursor **3a** produced material composed of 2.2% Fe, and dianion **4** gave a material with 1.9% Fe. These results correlate with the steric demands of the various precursors, suggesting that available surface area on the support surface is the key limitation to catalyst loading, and thus that precursor bulk is likely to be effective in separating individual precursor molecules on the surface. In all materials prepared below the maximum loadings, the Fe content closely matched the intended stoichiometry (Table 1, entries 4, 8, and 14), and grafting proceeded exactly as in those reactions involving more iron precursor than the surface would support.

Interestingly, neither the organic products nor the inorganic products of the grafting reactions were affected by the extent of hydroxyl coverage on the SBA-15 (Table 1, entries 2 vs. 3, 5 vs. 6, and 11 vs. 12). Most experiments were conducted using SBA-15 that had been calcined under oxygen at 770 K, then dried under vacuum to yield materials with hydroxyl group densities of 1.0–1.4 SiOH/nm^2 (as measured by both $(THF)_2Mg(Bn)_2$ [70] and TGA [71]). When this material was rehydroxylated in water (RT, 24 h) and dried at 390 K under N_2, silica featuring hydroxyl densities of 3.3–3.8 SiOH/nm^2 (and modestly lower surface areas) was obtained [74]. Grafting experiments using these hydroxylated silica samples were indistinguishable (by NMR and TGA) from those involving silica with lower OH concentrations. Furthermore, the loadings, catalytic activities, and

spectroscopic characteristics of the resulting materials were unaffected by the silica's hydroxyl content.

TGA analysis of all supported samples showed a smooth decrease in weight corresponding to the loss of >90% of organic components within 2 h of heating at 570 K under oxygen (Fig. 1). Thermolyses performed under nitrogen were less reproducible and produced variable weight losses corresponding to 50–80% of organic material. Bulk-scale calcination of **2–4-SBA15$_{295}$** was conducted at 570 K under oxygen for 2 h, and afforded catalysts **2–4-SBA15$_{573}$** (Table 2). All featured C < 1.0% and H < 0.5% (N undetectable). After calcination, the maximum iron loadings were measured as 3.4%, 2.4%, and 2.2% Fe for **2-**, **3a-**, and **4-SBA15$_{573}$**, respectively. Additional calcination at 570 K did not remove residual traces of carbon (entries 1 vs. 2). Although calcination at higher temperatures did lower the level of residual carbon, as discussed below, it also resulted in much less active catalytic materials (entry 7). Calcination at lower temperatures also resulted in somewhat reduced catalytic activity and elevated carbon content (entries 5 vs. 6). In all materials, the calcined catalyst suffered a 10–15% decline in surface area relative to the untreated support.

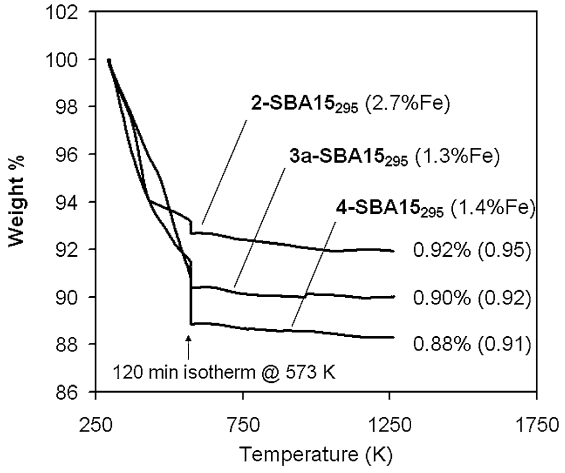

Fig. 1. TGA traces for the thermolyses of grafted materials **2-**, **3a-**, **4-SBA15$_{295}$** under O_2 (5 K/min, held at 573 K for 120 min) with actual (and theoretical) ceramic yields.

3.2. Spectroscopic characterization

To assess the structural changes associated with the synthetic steps described above, the materials were characterized using an array of spectroscopic techniques at each stage of catalyst preparation. Infrared spectroscopy demonstrated the disappearance of most organic C–H and C–C stretches on calcination of **2–4-SBA15$_{295}$**, but provided no other useful information regarding catalyst structure. The diffuse–reflectance ultraviolet–visible (DRUV) spectra of all supported, uncalcined materials showed a significant blue shift relative to the corresponding molecular precursors, and the spectra of the materials shifted only slightly on calcination (Fig. 2). No materials showed significant absorption maxima near 30,000 cm^{-1}, clearly demonstrating the absence of iron oxide clusters of significant size [29,75,76]. The maxima observed (ca. 39,000 cm^{-1}) were quite similar to those previously reported for monoiron materials 1-SBA15 (ca. 40,000 cm^{-1}), attributed to ligand–metal charge transfer to the iron center [60].

EPR spectra (recorded at room temperature) also showed significant differences between the precursor complexes and the corresponding supported materials (Fig. 3). Both Fe(III) precursors exhibit a major resonance near $g = 5$ (**3a**: $g = 5.1$; **4a**: $g = 4.7$) and a much weaker signal at $g = 2.0$. The former signal is generally attributed to tetrahedral sites with rhombic distortion, whereas the latter can arise from iron atoms in either tetrahedral or octahedral environments [77–79]. The Fe(II) precursor **2**, as expected for any Fe(II) species at room temperature, shows no significant resonance. After grafting, both **3-SBA15$_{295}$** and **4-SBA15$_{295}$** exhibited signals at $g = 4.3$ and 2.0, and **2-SBA15$_{295}$** showed very weak signals at these same values. All the EPR spectra of the calcined materials featured somewhat intensified $g = 2$ peaks, and in no case did the materials investigated exhibit the $g = 2.2$–2.5 signal associated with small iron oxide domains [77–79]. While it is hard to infer much more structural information from the resonances detected, all of these observations closely parallel previously reported results for many other supported iron centers, including the Fe/SBA-15 catalyst prepared using monoiron siloxide precursor **1a** [29,78,80].

Table 2
Effects of calcination time and temperature on catalyst performance[a]

Entry	Catalyst precursor	Fe (nm^{-2})	Initial SA (m^2/g)	Calc. time (h)	Calc. T (K)	%C	%Fe	Final SA (m^2/g)	Benzene TON, 1 h
1	**2**	0.19	650	2	573	0.86	1.55	600	13
2	**2**	0.19	650	5	573	0.82		580	11
3	**3a**	0.16	800	2	573	0.90	1.34	710	14
4	**3a**	0.16	800	0.5	573	2.90		750	12
5	**4**	0.16	825	2	573	1.04	1.38	745	22
6	**4**	0.16	825	5	423	1.72		690	15
7	**4**	0.16	825	2	773	0.79		660	6

[a] All catalysts were calcined under a flow of oxygen (100 mL/min), the calcination times indicated refer to the time at the listed temperature after ramping from room temperature at 5 K/min. TON are for the conversion of benzene to phenol using 50 mg catalyst, 22.4 mmol benzene, 5 mL CH_3CN, 4.0 mmol H_2O_2 at 333 K.

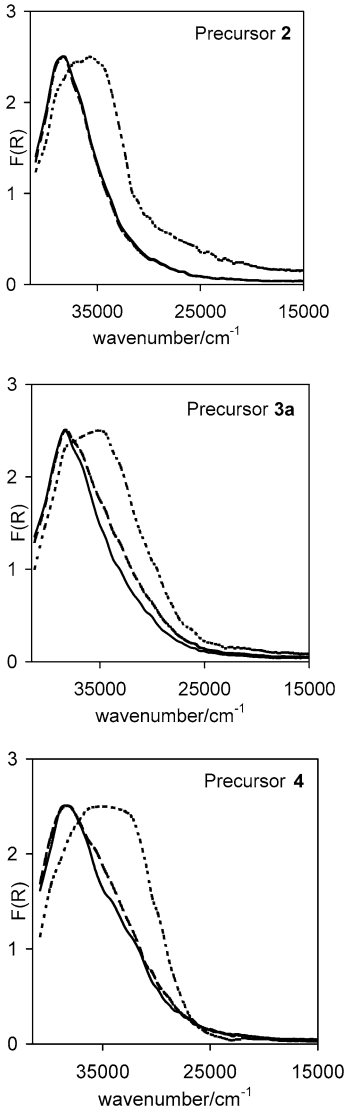

Fig. 2. DRUV spectra of precursors (···), grafted materials (- - -), calcined materials (—).

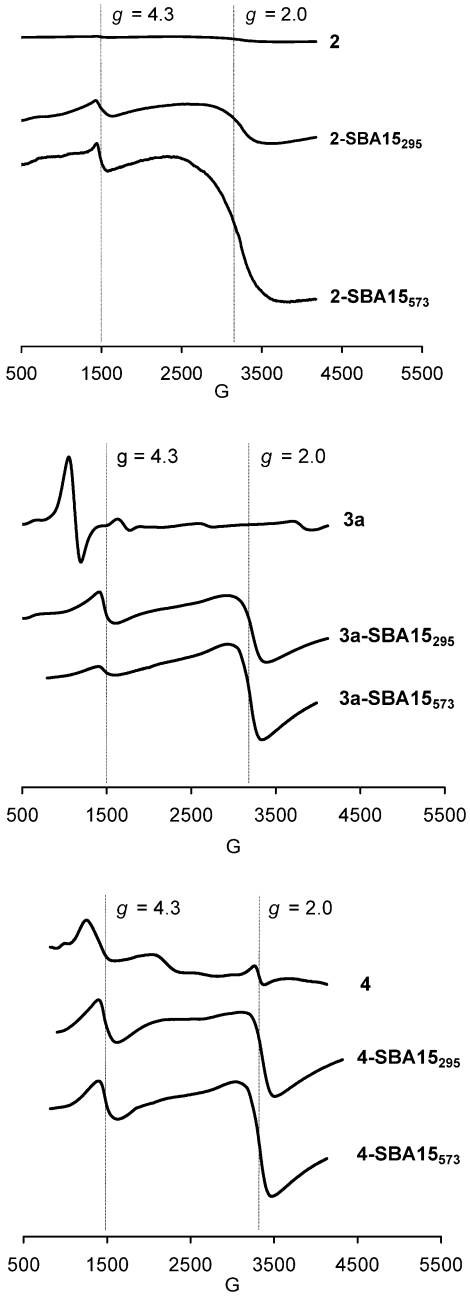

Fig. 3. EPR spectra of precursors, grafted materials, calcined materials.

Investigations using Mössbauer spectroscopy also exhibited striking similarities among the catalytic materials prepared from precursors **1**–**4** (Fig. 4, Table 3). With the exception of **2**, all iron(III) precursors (**1a**, **3a**, and **4**) yielded similar Mössbauer spectra featuring both isomer shift ($\delta =$ 0.38–0.43 mm/s) and quadrupole splitting values ($\Delta E_Q =$ 0.71–0.97 mm/s) consistent with the presence of iron(III) in a somewhat distorted high-spin environment (see Table 3, entries 1–3; Fig. 4, spectrum (a)) [81–84]. Compound **2** is unique in that it consists of approximately two-thirds high-spin iron(II), as is indicated by its very different hyperfine parameters [85], and approximately one-third high-spin iron(III). The spectrum of **2** showed evidence for multiple iron electronic environments (entry 4, spectrum (b)), suggesting that this highly air-sensitive compound was not stable enough to permit acquisition of its Mössbauer spectra before at least partial oxidation. The different components are shown for **2** in spectrum (b) of Fig. 4, and the resulting hyperfine parameters are listed in entry 4 of Table 3. It is worth noting that NMR, EA, and EPR studies all confirm the initial purity of this precursor before preparation of the Mössbauer spectral absorbers.

Unfortunately, because of the nature of the iron(III) quadrupole splitting, which arises only from the lattice contribution to the electric field gradient experienced by the iron-57 nucleus, it is difficult to draw definite conclusions about the differences in the local symmetry of the iron(III) in the different compounds. However, the observed line widths of 0.5–0.7 mm/s are quite large and indicate, as expected, that the iron(III) ions in a given compound experience a variety of slightly different local coordination environments.

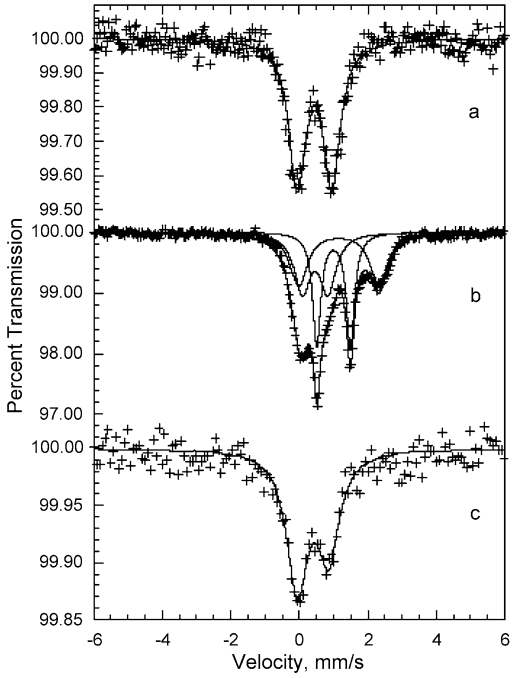

Fig. 4. The Mössbauer spectra of **4** (a), **2** (b), **4-SBA$_{573}$** (c), obtained at 77 K.

Table 3
Mössbauer spectral hyperfine parameters obtained at 77 K

Entry	Compound	δ[a] (mm/s)	ΔE_Q (mm/s)	Γ (mm/s)	Area (%)	Assignment
1	**1**	~0.43	~0.97	~0.51	100	distorted high-spin iron(III)
2	**3a**	0.38	0.92	0.70	100	distorted high-spin iron(III)
3	**4**	0.42	0.71	0.51	100	high-spin iron(III)
4	**2**	1.15	2.35	0.61	34	six-coord. high-spin iron(II)
		1.00	0.98	0.29	34	lower-coord. high-spin iron(II)
		0.46	0.76	0.55	32	high-spin iron(III)
5	**1-SBA15$_{573}$**	~0.43	~1.0	~0.7	100	distorted high spin iron(III)
6	**2-SBA15$_{573}$**	0.44	1.01	0.58	100	distorted high-spin iron(III)
7	**4-SBA15$_{573}$**	0.34	1.13	0.75	100	distorted high-spin iron(III)

[a] The isomer shifts are given relative to room temperature α-iron foil.

The Mössbauer spectral hyperfine parameters for the supported materials **1-**, **2-**, and **4-SBA15$_{573}$** (entries 5–7 of Table 3 and spectrum (c) of Fig. 5) differ only slightly from those of the precursors and have isomer shifts of 0.34–0.44 mm/s and quadrupole splittings of 1.0–1.1 mm/s—parameters that correspond more closely to those of neutral precursors **1** and **3a** than to dianion **4** or dimer **2**. The slightly larger quadrupole splittings evident in the spectra of the supported materials suggest that they likely feature greater distortions from tetrahedral geometry than do the precursor molecules. Both **2-** and **4-SBA15$_{573}$** are essentially indistinguishable from **1-SBA15$_{573}$** based on their Mössbauer spectra, although the uniformity of the Mössbauer spectra obtained for widely differing precursors suggests that this is likely due to fundamental limitations of the technique in distinguishing between similar, but not identical iron(III) sites.

Inspection of the EXAFS spectra (not corrected for phase shift) collected for materials derived from precursors **1**, **2**, and **4** offers insight into the relationships between the structures of the materials investigated (Fig. 5). The precursor molecules had very distinct scattering patterns. After grafting, however, **2-SBA15$_{295}$** exhibited a scattering pattern essentially identical to that of **1a-SBA15$_{295}$** obtained from monoiron precursor **1a**. After calcination, all materials prepared from precursors **1**–**4** were indistinguishable by visual inspection of their respective scattering patterns. The similarity exists not only in their amplitude parts, but also in their imaginary parts. All of the FT $k^3\chi(k)$ patterns exhibit a strong feature corresponding to Fe–O backscattering ($R = 1.3$–1.4 Å) and a weaker peak attributed to the second-shell Fe–Si scattering ($R = 2.7$–2.8 Å). Analysis of the imaginary component of the latter peak supports its attribution to Fe–Si scattering rather than to Fe–Fe scattering [36,61].

3.3. Catalysis

The materials prepared from precursors **2**–**4** were investigated as catalysts for selected solution phase hydrocarbon oxidation reactions and compared with the monoiron materials prepared from precursor **1a**. Activities and selectivities of **1a-SBA15$_{573}$** have been reported previously [60], but those reported in Tables 2 and 4 were measured concurrently with catalysts **2-**, **3-**, and **4-SBA15$_{573}$** to minimize differences arising from subtly varied preparative and catalytic procedures. Our studies revealed that the activity of all of the catalysts investigated is very sensitive to exposure of the catalyst to traces of water before substrate addition. Consequently, the data reported for **1a-SBA15$_{573}$** in Tables 2 and 4 show higher activities and markedly different selectivities than those reported previously [60]. The sensitivity of these reactions to reaction conditions will be discussed in a future publication [61].

Catalysts **2-, 3-**, and **4-SBA15$_{573}$** all showed significant activity for the hydroxylation of arenes with $H_2O_{2(aq)}$ (Table 4),

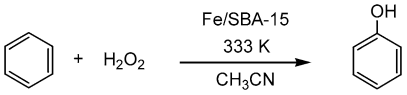

(4)

In this and in all solution phase oxidations, the dianion-derived catalyst **4-SBA15$_{573}$** was found to be the most active catalyst among samples with moderate, comparable iron loadings (Table 4). However, all catalysts, including monoiron material **1-SBA15$_{573}$**, were found to vary in activity by no more than a factor of 2. These results thus fall within the range of variability for multiple experiments conducted on different occasions or using different batches of a given

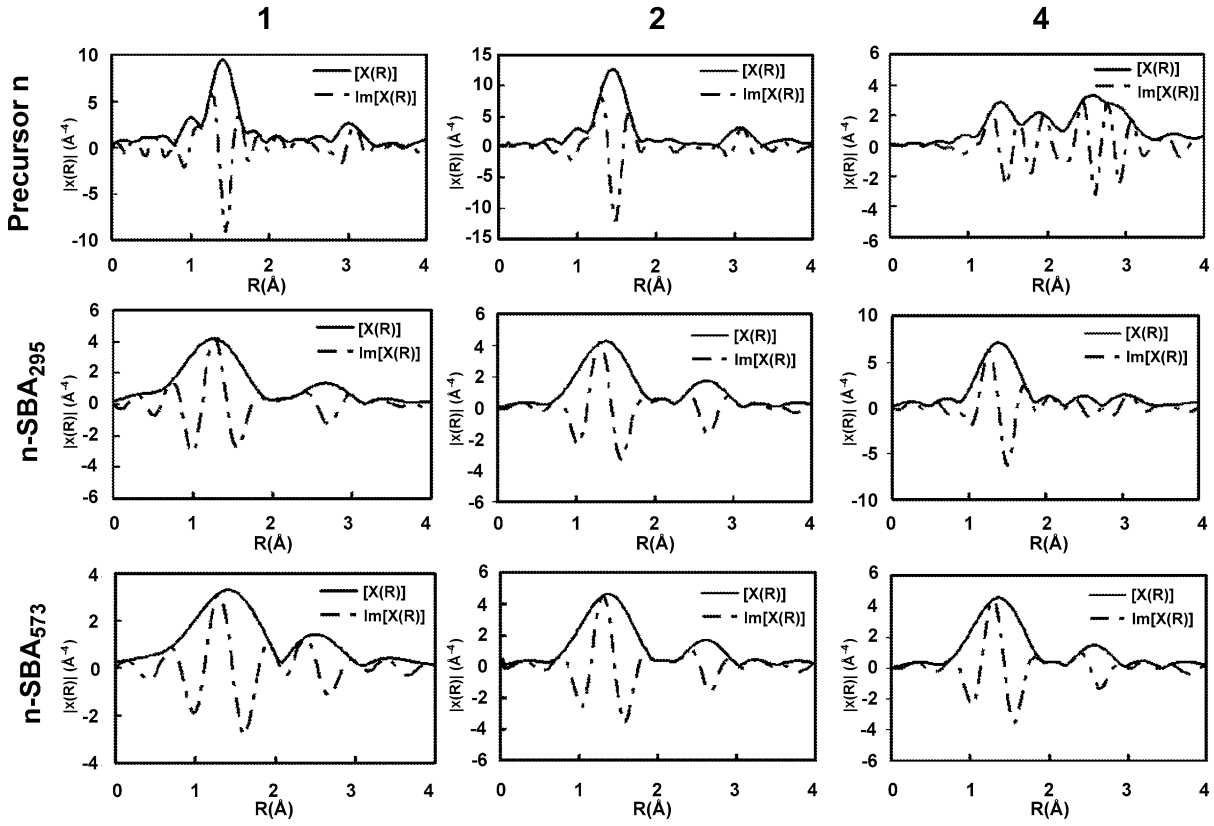

Fig. 5. k^3-weighted Fourier transformation of Fe K-edge XAS data for precursors, grafted materials, calcined materials derived from precursors **1**, **2**, **4**. The imaginary parts of Fourier transformed data are plotted as dash dot lines.

Table 4
Solution-phase catalytic activity and selectivity[a]

Entry	Catalyst	Fe (nm^2)	Toluene oxidation		Adamantane oxidation			Cyclohexene oxidation	
			TON, 1 h	sp^2/sp^3	TON, 1 h	3°/2°[b]	One/ol	% oxide	One/ol
1	**1-SBA15$_{573}$**	0.17	13	3.8	10	1.8	1.6	0	1.5
2	**2-SBA15$_{573}$**	0.19	12	3.6	12	2.3	1.5	1	1.3
3	**2-SBA15$_{573}$**	0.07	20	3.4	15	2.4	1.6	1	1.6
4	**3a-SBA15$_{573}$**	0.18	13	3.4	12	2.2	1.5	2	1.4
5	**3b-SBA15$_{573}$**	0.05	19	3.5	19	2.3	1.7	4	1.6
6	**4-SBA15$_{573}$**	0.18	15	3.7	14	1.9	1.4	1	1.4
7	**4-SBA15$_{573}$**	0.04	49	3.2	34	2.1	1.7	2	1.5

[a] All catalysts were prepared using standard conditions, including calcination for 2 h at 573 K. Reaction conditions: substrates 10.5–22.4 mmol, catalyst 50 mg (13–14 mmol Fe), H_2O_2 4 mmol, CH_3CN 5 mL, reaction time 1 h. Reaction temperature 295–333 K, dodecane (internal standard) 214 μmol.

[b] The sp^2/sp^3 ratio describes the selectivity for oxidation at sp^2 hybridized aryl carbons (to produce cresol) vs. the sp^3 hybridized benzylic position (to produce benzyl alcohol and benzaldehyde).

catalyst. Toluene (Eq. (5)) was oxidized selectively at aryl C–H bonds to yield *o*- and *p*-phenol, although substantial benzaldehyde was also formed (sp^2/sp^3 selectivity ≈3.5). Benzyl alcohol was produced in only trace quantities. The product selectivities varied less among various materials than between different runs with the same catalyst [86].

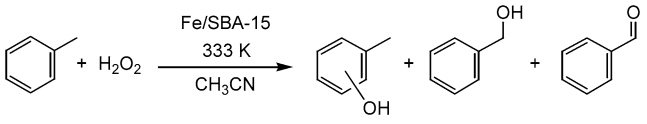

(5)

All of the catalysts investigated convert adamantane to a mixture of the corresponding tertiary alcohol, secondary alcohol, and ketone (Eq. (6)),

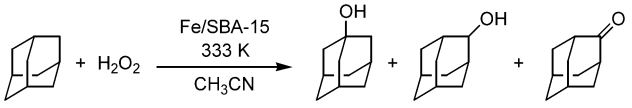

(6)

Their selectivities for oxidizing the weaker, tertiary C–H bond were at the low end of those recorded (1.8–2.4) and were fairly consistent among all of the catalysts investigated. The ratio of ketone to alcohol formation in oxidation at sec-

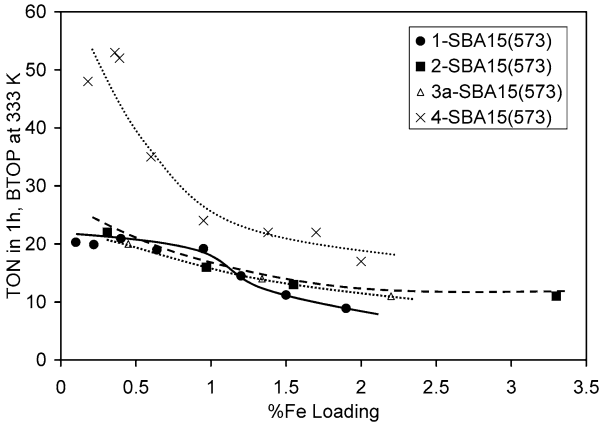

Fig. 6. Dependence of activity upon Fe-loading for benzene oxidation by catalysts **1-**, **2-**, **3a-**, **4-SBA15$_{573}$**.

ondary C–H bonds varied from 1.4 to 1.7, but again this variation among catalysts does not exceed the range of inherent variability in these reactions. Oxidation of cyclohexene (Eq. (7))

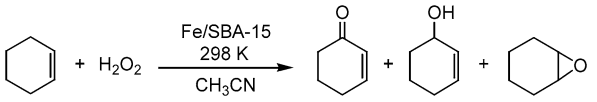

(7)

resulted almost exclusively in slow oxidation at the allylic position (TON values between 0 and 4) rather than epoxide formation, and this selectivity varied little among the catalysts investigated.

Catalyst activity was found to depend on the iron loading, as illustrated in Fig. 6 for the oxidation of benzene to phenol. All catalysts showed moderately higher per-iron activity at lower loadings, with **4-SBA15$_{573}$** exhibiting the most striking dependence. It is noteworthy, however, that the higher activities of these iron-poor catalysts were not accompanied by changes in selectivity or spectroscopic features (DRUV, EPR).

Very little leaching was observed over 1–2 h of catalysis. For catalysts **2-, 3-**, and **4-SBA15$_{573}$**, the reaction solution slowly turned a pale yellow color (visible after 1 h), but when separated from the solid catalyst it showed no catalytic activity. Catalyst **4-SBA15$_{573}$** recovered after 2 h and recalcined exhibited activity comparable to that observed initially.

4. Discussion

The diiron molecular precursors investigated were designed to satisfy several criteria. Foremost among these was the requirement that they have the same –OSi(O^{t}Bu)$_3$ ligand that facilitated controlled grafting chemistry and clean calcination in the previously reported monoiron system [60]. Additionally, commensurate with the goal of preparing a strictly inorganic material under mild conditions, large organic ligands were avoided. Finally, to the extent compatible with the first two requirements, structures featuring iron–iron linkages similar to known diiron oxidation catalysts (featuring μ–oxo and μ–hydroxo diiron centers) were designed.

Diiron dimer [Fe(OSi(O^{t}Bu)$_3$)$_2$]$_2$ (**2**), prepared by a well-precedented protonolysis method (Eq. (1)), is similar to the known, structurally characterized analogs featuring other siloxide [87] and silylsulfide [88] ligands. The dimeric solution structure of **2** was confirmed by both ^{1}H NMR spectroscopy (δ 5.21 (br), −11.13 (br) ppm, corresponding to the bridging and terminal siloxide groups, respectively) and solution molecular weight measurements in pentane (MW Calcd: 1164. Found: 1140). Efforts to convert this species to a μ–oxo diiron structure through oxidation (as has been achieved with other Fe(II) species [89]) were unsuccessful; treatment of **2** with N_2O, O_2, PhIO, pyridine *N*-oxide, or trimethylamine *N*-oxide resulted exclusively in disproportionation to yield trisiloxide complex **1a** (or amine derivatives) and insoluble red material presumed to be a macromolecular oxide species. The Fe(II) complex **2** itself seemed to be a reasonable precursor for diiron sites, however. In addition to the requisite siloxide ligand, the complex features two μ–siloxide linkages similar to the μ–hydroxo moieties found in many MMO mimics. The smaller per-iron size of this precursor appears to allow it to be grafted at significantly higher weight loadings than those achieved with larger precursors **1**, **3**, **4**.

Complexes (**3a–c**), featuring bridging nitrogen ligands, were prepared most efficiently via treatment of the diethylether adduct Fe(OSi(O^{t}Bu)$_3$)$_3$(Et$_2$O) (**1b**) with the appropriate ligand (Eq. (2)), although they could also be prepared in much lower yield (38% vs. 89% for the TMEDA complex **3a**) by the treatment of THF adduct **1a** with ligand. The dinuclear structures of these complexes were verified by elemental analysis (1.55% N; 1.59% Calcd for **3a**, vs. 2.84% Calcd for monoiron adduct Fe[OSi(O^{t}Bu)$_3$]$_3$N(CH$_3$)$_2$–C$_2$H$_4$N(CH$_3$)$_2$) and measurement of the solution molecular weight of TMEDA complex **3a**. Although these precursors do not feature the desired linkage structure, they do have the advantage of having very robust iron–iron linkages unlikely to cleave during the grafting process.

Precursor **4**, prepared by a simple salt metathesis reaction (Eq. (3)), features a true μ–oxo diiron core. The characteristic μ–oxo stretch (observed for the starting material [Cl$_3$FeOFeCl$_3$][NEt$_4$]$_2$ at $\nu_{FeOFe} = 855$ cm^{-1}) was obscured in the infrared spectrum of precursor **4** by stronger bands arising from the siloxide ligands. But the dinuclear nature of **4** was supported by elemental analysis and by solution molecular weight determination. Modification of the reaction stoichiometry (NaOSi(O^{t}Bu)$_3$:[Cl$_3$FeOFeCl$_3$][NEt$_4$]$_2$ = 4:1 vs. 6:1), replacement of the countercation (Li, Na), and introduction of additional dative ligands (dioxane, pyridine) in this procedure did not induce formation of a neutral precursor of the type [(^{t}BuO)$_3$SiO]$_2$(L)FeOFe(L)[OSi(O^{t}Bu)$_3$]$_2$. Nonetheless, the μ–oxo linkage in precursor **4** makes it the most direct analog to the proposed diiron catalysts in both oxide-supported [4] and biological [8] systems. It is worth noting, however, that this catalyst precursor

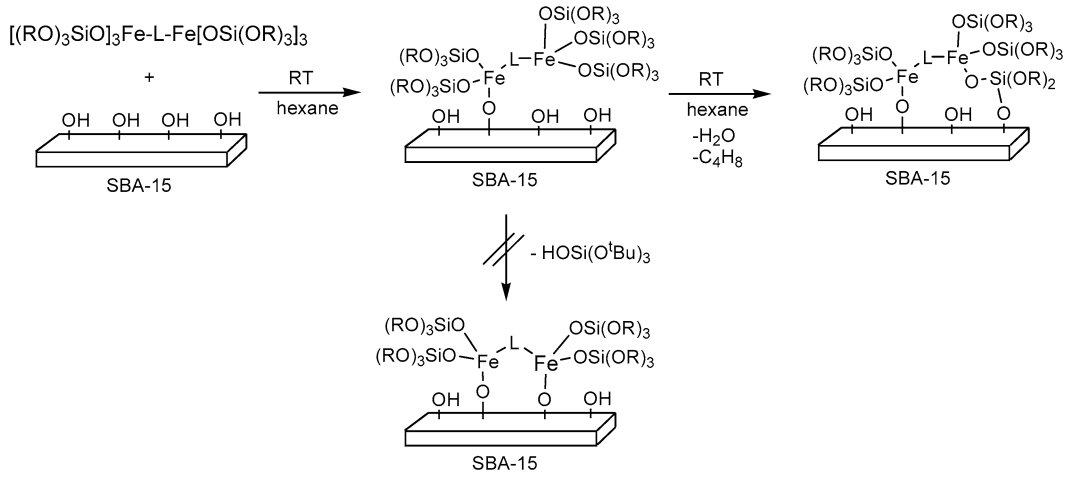

Scheme 2.

is tetrahedral rather than octahedral, which limits the usefulness of analogies drawn between these systems.

The different grafting stoichiometries among the catalysts suggest that the initial binding of the precursors to the support depends on the precursor structure. Treatment of complex **3** or **4** with SBA-15 results in the initial liberation of one equivalent of silanol per precursor complex, whereas precursor **2** produces two equivalents per diiron molecule. Given the spectroscopic evidence that catalysts derived from **2** resemble those prepared using monoiron precursor **1a** even *before* calcination, it appears likely that the liberation of one silanol group for every iron center is a result of dimer cleavage during the grafting process. Complexes **3** and **4** do not yield two full equivalents of silanol even after extended grafting times, but the formation of at least one equivalent of isobutylene suggests that a second grafting event indeed occurs. Because this is not observed in the grafting of monoiron precursor **1a**, it is possible that the second grafting event involves the second iron center (Scheme 2). Geometric constraints on the surface may favor this mode of grafting over silanol protonolysis at this iron center. The absence of free diamine ligand in the grafting reactions of precursors **3a–c** demonstrates that grafting does not occur through displacement of the linker and suggests that the diiron unit likely remains intact. Likewise, the generation of silanol in the grafting of **4** argues against cleavage of the Fe–O–Fe bond during the grafting process; protonolysis of this bond would initially generate water rather than silanol. Although we cannot rule out initial formation of water and its further reaction with precursor to generate the observed silanol, several observations argue against this possibility. No color change is observed (**4** darkens on exposure to water), the initial silanol generation is quite fast (the sterically protected Fe–O–Fe linkage would be expected to react slowly), and only a single equivalent of silanol is observed (one equivalent water could liberate two equivalents of silanol).

The spectroscopic data obtained from DRUV and EPR for materials of various loadings rule out the presence of iron oxide or iron clusters of significant size, demonstrating the general utility of siloxide precursors in preparing well-dispersed supported materials at iron weight loadings up to 3.4% Fe. However, neither these methods nor Mössbauer investigations provide data capable of distinguishing between monoiron and diiron(III) species on the support. The parameters collected from all of these spectroscopic methods are in keeping with typical supported iron(III) sites, most likely in a distorted tetrahedral environment. A cursory review of EXAFS data shows a striking similarity among all calcined materials prepared from precursors **1–4**, suggesting that the calcination process renders these catalysts indistinguishable. Uncalcined catalyst **2-SBA15$_{295}$** is indistinguishable from **1a-SBA15$_{295}$**, a finding consistent with the grafting results suggesting that this precursor actually cleaves during the grafting process. The FT $k^3\chi(k)$ of **3-** and **4-SBA15$_{295}$** contain unique features, as expected given the lack of any evidence for precursor cleavage during grafting. But it appears that no diiron linkage is formed during the calcination of **3a**, and that the preexisting μ-oxo linkage of precursor **4** is cleaved to yield two materials with isolated iron centers (Scheme 3) [90].

The hypothesis that calcination cancels the effect of precursor design is supported by the similarities among the catalytic activities and selectivities of the catalysts investigated [91]. Given the significant variability observed among catalysis runs, there is very little difference among the activities or selectivities of the diiron catalysts investigated, or between these catalysts and that derived from monoiron precursor **1a** (Table 4). Note, however, that all of these catalysts exhibited high activity in all of the reactions investigated. The selective oxidation of toluene to cresols, as well as the 3°/2° ratio of adamantane oxidation products and the absence of epoxide product for cyclohexene oxidation, are consistent with a mechanism involving •OH radicals or •OH radical sources [61,92–95].

Interestingly, all catalysts showed a significant dependence of per-iron activity on weight loading. Although such data are often interpreted to suggest the presence of different active sites at different loadings [96–100], in this case

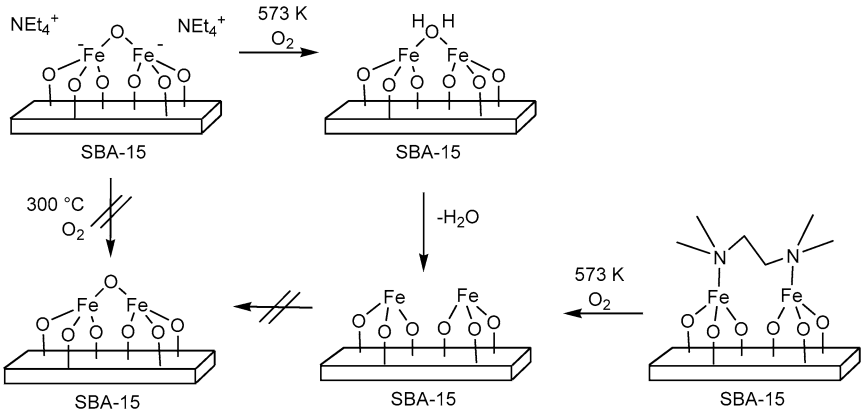

Scheme 3.

the activity differences were not mirrored by spectroscopic data or catalytic selectivity, making the explanation for this phenomenon less certain. It is possible that spectroscopically indistinguishable yet different active sites are present at lower loadings, although it is hard to imagine what species might be present at lower loadings if monoiron centers dominate even at the highest loadings used. Furthermore, it would be surprising for a change in structure to alter activity without affecting any of the wide array of selectivities measured.

Although the work described herein appears not to have yielded the targeted dinuclear iron catalyst after calcination, it does offer substantial insight regarding the relative stabilities of diiron and monoiron structures on silica. The grafting of two centers in close proximity appears to be difficult, because dimeric precursor **2** cleaves during grafting rather than placing two bridged iron centers on the support. Likewise, precursors **3** and **4** each undergo only one protonolysis reaction (Scheme 2), suggesting that the formation of a grafted, bridged geometry is sufficiently disfavored so to be not overcome by the enforced proximity of the support in the intermediate η-1 structure. The fully grafted precursors **3a–c** do not form μ–oxo linkages on calcination despite the enforced proximity of the iron centers, and the existing μ–oxo functionality in the grafting product of **4** is destroyed by calcination (Scheme 4). Furthermore, such structural changes on calcination are unlikely to be a consequence of iron mobility on the support; no evidence of bulk iron oxide is observed, although evidence in many related systems suggests agglomerization to be the ultimate result under conditions allowing for iron migration [34,43–46,62,101]. The simplest explanation for these observations is that for two adjacent iron centers on a silica support, the formation of a μ–oxo bridge is simply thermodynamically disfavored.

5. Conclusions

The grafting chemistry described herein provides further evidence of the generality of the molecular precursor approach. Various diiron siloxide complexes are synthetically accessible; each undergoes clean, simple, and non-aqueous grafting chemistry that can be readily monitored by NMR spectroscopy. In two of the precursors investigated, this grafting appears to yield a supported iron species very similar in structure to the molecular precursor. Although the precursors all yield catalysts active in the oxidation of hydrocarbons with H_2O_2, the precursor design has very little impact on the ultimate catalytic behavior or spectroscopic properties of the catalyst after calcination. These attempts to prepare inorganic diiron species on the support highlight a key limitation of the molecular precursor approach: Even under relatively mild calcination conditions, thermodynamic preferences may still overwhelm the influence of careful precursor design. Nonetheless, these results offer the important finding that diiron centers are neither readily generated nor preserved in the environment of a mesoporous silica support.

Acknowledgments

This work was supported by the Office of Energy Research, Office of Basic Energy Sciences, Chemical Sciences Division, U.S. Department of Energy (contract DE-AC03-76SF00098). We gratefully acknowledge Dr. Junko Yano for assistance with EPR measurements.

References

[1] V.I. Sobolev, K.A. Dubkov, O.V. Panna, G.I. Panov, Catal. Today 24 (1995) 251.
[2] G.I. Panov, A.K. Uriarte, M.A. Rodkin, V.I. Sobolev, Catal. Today 41 (1998) 365.
[3] L.J. Lobree, I.C. Hwang, J.A. Reimer, A.T. Bell, J. Catal. 186 (1999) 242.
[4] P. Marturano, L. Drozdova, A. Kogelbauer, R. Prins, J. Catal. 192 (2000) 236.
[5] R. Joyner, M. Stockenhuber, J. Phys. Chem. B 103 (1999) 5963.
[6] B.J. Wallar, J.D. Lipscomb, Chem. Rev. 96 (1996) 2625.
[7] T. Klabunde, B. Krebs, Struct. Bond. 89 (1997).
[8] S.J. Lange, L.J. Que, Curr. Opin. Chem. Biol. 2 (1998) 159.
[9] A.C. Rosenzweig, P. Nordlund, T.P.M.C.A. Frederick, S.J. Lippard, Chem. Biol. 2 (1995) 409.
[10] A.C. Rosenzweig, C.A. Frederick, S.J. Lippard, P. Nordlund, Nature 366 (1993) 537.

[11] N. Elango, R. Radhakrishnan, W.A. Frohland, B.J. Wallar, C.A. Earhart, J.D. Lipscomb, D.H. Ohlendorf, Protein Sci. 6 (1997).
[12] P.R. Ortiz de Montellano (Ed.), Cytochrom P450, Plenum, New York, 1986.
[13] R.H. Holm, P. Kennepohl, E.I. Solomon, Chem. Rev. 96 (1996) 2239.
[14] L. Que, R.Y.N. Ho, Chem. Rev. 96 (1996) 2607.
[15] G.H. Loew, D.L. Harris, Chem. Rev. 100 (2000) 407.
[16] M. Costas, M.P. Mehn, M.P. Jensen, L. Que, Chem. Rev. 104 (2004) 939.
[17] H. Arakawa, M. Aresta, J.N. Armor, M.A. Barteau, E.J. Beckman, A.T. Bell, E. Bercaw, C. Creutz, E. Dinjus, D.A. Dixon, K. Domen, D.L. DuBois, J. Eckert, E. Fujita, D.H. Gibson, W.A. Goddard, D.W. Goodman, J. Keller, G.J. Kubas, H.H. Kung, J.E. Lyons, L.E. Manzer, T.J. Marks, K. Morokuma, K.M. Nicholas, et al., Chem. Rev. 101 (2001) 953.
[18] F.A. Walker, Chem. Rev. 104 (2004) 589.
[19] M.H. Baik, M. Newcomb, R.A. Friesner, S.J. Lippard, Chem. Rev. 103 (2003) 2385.
[20] H.-F. Hsu, Y. Dong, L. Shu, V.G.J. Young, L.J. Que, J. Am. Chem. Soc. 121 (1999) 5230.
[21] L. Westerheide, M. Pascaly, B. Krebs, Curr. Opin. Chem. Biol. 4 (2000) 235.
[22] A.M. Valentine, S.S. Stahl, S.J. Lippard, J. Am. Chem. Soc. 121 (1999) 3876.
[23] V. Schunemann, A.X. Trautwein, I. Rietjens, M.G. Boersma, C. Veeger, D. Mandon, R. Weiss, K. Bahl, C. Colapietro, M. Piech, R.N. Austin, Inorg. Chem. 38 (1999) 4901.
[24] K. Neimann, R. Neumam, A. Rabion, R.M. Buchanan, R.H. Fish, Inorg. Chem. 38 (1999) 3575.
[25] D.W. Lewis, G. Sankar, C. Richard, C.R.A. Catlow, S.W. Carr, J.M. Thomas, Nucl. Instr. Meth. Phys. Res. B: Beam Interact. Mater. Atoms 97 (1995) 44.
[26] J.A. Ryder, A.K. Chakraborty, A.T. Bell, J. Catal. 220 (2003) 84.
[27] A.R. Overweg, M.W.J. Craje, I. Arends, A.M. van der Kraan, Hyperfine Interact. 141 (2002) 391.
[28] J. Perez-Ramirez, G. Mul, F. Kapteijn, J.A. Moulijn, A.R. Overweg, A. Domenech, A. Ribera, I. Arends, J. Catal. 207 (2002) 113.
[29] A. Ribera, I. Arends, S. de Vries, J. Perez-Ramirez, R.A. Sheldon, J. Catal. 195 (2000) 287.
[30] S.J. Ma, L.S. Li, F.P. Sun, S.L. Qiu, Chem. J. Chin. Univ. 18 (1997) 504.
[31] N.S. Ovanesyan, A.A. Shteinman, K.A. Dubkov, V.I. Sobolev, G.I. Panov, Kinet. Catal. 39 (1998) 792.
[32] R.Q. Long, R.T. Yang, J. Catal. 194 (2000) 80.
[33] N.H. Phu, T.T.K. Hoa, N. Van Tan, H.V. Thang, P. Le Ha, Appl. Catal. B 34 (2001) 267.
[34] K.A. Dubkov, N.S. Ovanesyan, A.A. Shteinman, E.V. Starokon, G.I. Panov, J. Catal. 207 (2002) 341.
[35] E.J.M. Hensen, Q. Zhu, M. Hendrix, A.R. Overweg, P.J. Kooyman, M.V. Sychev, R.A. van Santen, J. Catal. 221 (2004) 560.
[36] S.H. Choi, B.R. Wood, J.A. Ryder, A.T. Bell, J. Phys. Chem. B 107 (2003) 11843.
[37] A.A. Battiston, J.H. Bitter, D.C. Koningsberger, Catal. Lett. 66 (2000) 75.
[38] P. Coquay, R.E. Vandenberghe, E. De Grave, A. Fonseca, P. Piedigrosso, J.B. Nagy, J. Appl. Phys. 92 (2002) 1286.
[39] P. Fejes, K. Lazar, I. Marsi, A. Rockenbauer, L. Korecz, J.B. Nagy, S. Perathoner, G. Centi, Appl. Catal. A 252 (2003) 75.
[40] K. Lazar, A.N. Kotasthane, P. Fejes, Catal. Lett. 57 (1999) 171.
[41] A.V. Kucherov, C.N. Montreuil, T.N. Kucherova, M. Shelef, Catal. Lett. 56 (1998) 173.
[42] Q. Zhu, B.L. Mojet, R.A.J. Janssen, E.J.M. Hensen, J. van Grondelle, P. Magusin, R.A. van Santen, Catal. Lett. 81 (2002) 205.
[43] Y. Kurusu, D.C. Neckers, J. Org. Chem. 56 (1991) 1981.
[44] R.L. McCormick, G.O. Alptekin, D.L. Williamson, T.R. Ohno, Top. Catal. 10 (2000) 115.
[45] T. Tagawa, Y.J. Seo, S. Goto, J. Mol. Catal. 78 (1993) 201.
[46] U. Schuchardt, R. Pereira, C.E.Z. Krahembuhl, M. Rufo, R. Buffon, Appl. Catal. 131 (1995) 135.
[47] V.I. Sobolev, K.A. Dubkov, O.V. Panna, G.I. Panov, Catal. Today 24 (1995) 251.
[48] Y. Yamada, Y. Ichihashi, H. Ando, A. Ueda, H. Shioyama, T. Kobayashi, Chem. Lett. 32 (2003) 208.
[49] J.M. Thomas, Top. Catal. 15 (2001) 85.
[50] R.K. Grasseli, Top. Catal. 15 (2001) 93.
[51] J.-C. Volta, Top. Catal. 15 (2001) 121.
[52] J.-M.M. Millet, J.C. Vedrine, Top. Catal. 15 (2001) 139.
[53] C. Rosier, G.P. Niccolai, J.M. Basset, J. Am. Chem. Soc. 119 (1997) 12408.
[54] V.R. Dufaud, J.M. Basset, Angew. Chem. Int. Ed. 37 (1998) 806.
[55] M. Chabanas, V. Vidal, C. Coperet, J. Thivolle-Cazat, J.M. Basset, Angew. Chem. Int. Ed. 39 (2000) 1962.
[56] J. Guzman, B.C. Gates, Langmuir 19 (2003) 3897.
[57] G.L. Rice, S.L. Scott, Langmuir 13 (1997) 1545.
[58] K.L. Fujdala, T.D. Tilley, J. Catal. 216 (2003) 265.
[59] D.Y. Zhao, Q.S. Huo, J.L. Feng, B.F. Chmelka, G.D. Stucky, J. Am. Chem. Soc. 120 (1998) 6024.
[60] C. Nozaki, C.G. Lugmair, A.T. Bell, T.D. Tilley, J. Am. Chem. Soc. 124 (2002) 13194.
[61] G.T. Li, A.T. Bell, T.D. Tilley, manuscript in preparation.
[62] Y. Yamada, A. Ueda, K. Nakagawa, T. Kobayashi, Res. Chem. Intermed. 28 (2002) 397.
[63] H. Hayashi, L.Z. Chen, T. Tago, M. Kishida, K. Wakabayashi, Appl. Catal. A 231 (2002) 81.
[64] M.C. White, A.G. Doyle, E.N. Jacobsen, J. Am. Chem. Soc. 123 (2001) 7194.
[65] L. Que, Y.H. Dong, Acc. Chem. Res. 29 (1996) 190.
[66] R.A. Andersen, K. Faegri, J.C. Green, A. Haaland, M.F. Lappert, W.-P. Leung, K. Rypdal, Inorg. Chem. 27 (1988) 1782.
[67] Y. Abe, I. Kijima, Bull. Chem. Soc. Jpn. 42 (1969) 1118.
[68] A.K. McMullen, T.D. Tilley, A.L. Rheingold, S.J. Geib, Inorg. Chem. 28 (1989) 3772.
[69] W.H. Armstrong, S.J. Lippard, Inorg. Chem. 24 (1985) 981.
[70] K.L. Fujdala, T.D. Tilley, J. Am. Chem. Soc. 123 (2001) 10133.
[71] R. Mueller, H.K. Kammler, K. Wegner, S.E. Pratsinis, Langmuir 19 (2003) 160.
[72] R.W. Zoellner, J. Chem. Educ. 67 (1990) 714.
[73] R. Signer, Justus. Liebig. Ann. Chem. 478 (1930) 246.
[74] L.T. Zhuravlev, Colloids Surf. A: Physicochem. Eng. Aspects 173 (2000) 1.
[75] S. Bordiga, R. Buzzoni, F. Geobaldo, C. Lamberti, E. Giamello, A. Zecchira, G. Leofanti, G. Petrini, G. Tozzola, G. Vlaic, J. Catal. 158 (1996) 486.
[76] H.H. Tippins, Phys. Rev. B 1 (1970) 126.
[77] P. Selvam, S.E. Dapurkar, S.K. Badamanli, M. Muragasam, H. Kuwano, Catal. Today 68 (2001) 69.
[78] D. Goldfarb, M. Bernard, K.G. Strohmainer, D.E.W. Vaughan, H. Thomann, J. Am. Chem. Soc. 116 (1994) 6344.
[79] B.M. Wechuysen, D. Wang, M.P.R. Rosynek, J.H. Lunsford, Angew. Chem., Int. Ed. Engl. 36 (1997) 2374.
[80] W.A. Carvalho, M. Wallau, U. Schuchardt, J. Mol. Catal. A 144 (1999) 91.
[81] W.M. Reiff, G.J. Long, W.A. Baker Jr., J. Am. Chem. Soc. 90 (1968) 6347.
[82] J.A. Bertrand, J.L. Breece, A.R. Kalyanaraman, G.J. Long, W.A. Baker Jr., J. Am. Chem. Soc. 92 (1970) 5233.
[83] G.J. Long, J.T. Wrobleski, R.V. Thundathil, D.M. Sparlin, E.O. Schlemper, J. Am. Chem. Soc. 102 (1980) 6040.
[84] S. Tanase, E. Bouwman, G.J. Long, A.M. Shahin, R. de Gelder, A.M. Mills, A.L. Spek, J. Reedijk, Polyhedron, in press.
[85] W.M. Reiff, G.J. Long, in: G.J. Long (Ed.), Mössbauer Spectroscopy and the Coordination Chemistry of Iron, in Mössbauer Spectroscopy Applied to Inorganic Chemistry, vol. 1, Plenum, New York, 1984, p. 245.

[86] Representative experiments (analogous to entries 2 and 6 in Table 4) indicate that substrate oxidation accounts for approximately 80% of total peroxide consumption (as measured by Raman Spectroscopy). The issue of hydrogen peroxide selectivity will be addressed in greater detail in a future publication [61].

[87] T.A. Chesnokova, E.V. Zhezlova, A.N. Kornev, Y.V. Fedotova, L.N. Zakharov, G.K. Fukin, Y.A. Kursky, T.G. Mushtina, G.A. Domrachev, J. Organomet. Chem. 642 (2002) 20.

[88] T. Komuro, H. Kawaguchi, K. Tatsumi, Inorg. Chem. 41 (2002) 5083.

[89] P. Giancnoccaro, E. Pannacciulli, F. Morazzoni, A. Gervasini, Gazz. Chim. Ital. 116 (1986) 147.

[90] No data is available regarding the order of the steps depicted in Scheme 3; it is meant only to illustrate that both removal of organic components and linker cleavage occur during this process.

[91] Unfortunately, catalytic experiments using uncalcined materials (possibly containing diiron units) invariably resulted in extensive leaching and homogeneous catalysis marked by dramatically darkened reaction mixtures, high reaction rates, and extremely poor reaction selectivity. This is not surprising given the fragility of the linkage between support and metal in these complexes.

[92] P. Stavropoulos, R. Celenligil-Cetin, A.E. Tapper, Acc. Chem. Res. 34 (2001) 745.

[93] R.A. Sheldon, M. Wallau, I. Arends, U. Schuchardt, Acc. Chem. Res. 31 (1998) 485.

[94] S. Goldstein, D. Meyerstein, Acc. Chem. Res. 32 (1999) 547.

[95] D.T. Sawyer, A. Sobkowiak, T. Matsushita, Acc. Chem. Res. 29 (1996) 409.

[96] M. Puglisi, F. Arena, F. Frusteri, V. Sokolovskii, A. Parmaliana, Catal. Lett. 41 (1996) 41.

[97] T. Tanaka, K. Teramura, T. Yamamoto, S. Takenaka, S. Yoshida, T. Funabiki, J. Photochem. Photobiol. A: Chem. 148 (2002) 277.

[98] Q.H. Xia, K. Hidajat, S. Kawi, J. Catal. 205 (2002) 318.

[99] G. Xiong, C. Li, Z.C. Feng, P.L. Ying, Q. Xin, J.K. Liu, J. Catal. 186 (1999) 234.

[100] C.H. Kim, W.L. Yoon, I.C. Lee, S.I. Woo, Appl. Catal. A 144 (1996) 159.

[101] P. Ratnasamy, R. Kumar, Catal. Today 9 (1991) 328.